ELSEVIER

Journal of Neuroscience Methods 158 (2006) 50–55

JOURNAL OF NEUROSCIENCE METHODS

www.elsevier.com/locate/jneumeth

Manganese-enhanced 3D MRI of established and disrupted synaptic activity in the developing insect brain in vivo

Takashi Watanabe [a,*], Joachim Schachtner [b], Mojmir Krizan [a], Susann Boretius [a], Jens Frahm [a], Thomas Michaelis [a]

[a] *Biomedizinische NMR Forschungs GmbH, Max-Planck-Institut für biophysikalische Chemie, 37070 Göttingen, Germany*
[b] *Fachbereich Biologie, Tierphysiologie, Philipps-Universität, Marburg, Germany*

Received 12 January 2006; received in revised form 3 May 2006; accepted 5 May 2006

Abstract

The antennal lobe of the sphinx moth *Manduca sexta* serves as a model for the development of the olfactory system. Here, the establishment of the glomerular synaptic network formed by the olfactory receptor axons and antennal lobe neurons at pupal stage P12 was followed by transection of the right antenna and – within 24 h – by injection of $MnCl_2$ into the hemolymph. In vivo 3D MRI at 100 and 60 μm isotropic resolution was then performed at P13 to P17. Whereas the left antennal lobe revealed a pronounced increase of the signal-to-noise ratio (SNR) reflecting normal synaptic activity, the observation of only a small SNR increase within the right antennal lobe indicated the disruption of pertinent activity after antennal transection. The accumulation of manganese in the intact antennal system became observable within 3 h and lasted for at least 2 days after injection. Intra-individual comparisons between the right and left side yielded a statistically significant differential SNR increase in the left antennal lobe. Because such an effect was not observed in younger animals studied at pupal stages P10/P11, the MRI findings confirm the development of functional synapses in the antennal lobe of *Manduca sexta* by P13.

Keywords: Magnetic resonance imaging; Manganese; Brain; Entomology; *Manduca sexta*; Antennal lobe

1. Introduction

Manganese-enhanced MRI is increasingly used for a functional characterization of the central nervous system of rodents (e.g., see Koretsky and Silva, 2004; Pautler, 2004; Watanabe et al., 2004). Scarce applications to other species include non-human primates, birds, and crayfish as invertebrates (Herberholz et al., 2004; Brinkley et al., 2005). The technique relies upon the activity-dependent neuronal uptake of paramagnetic manganese ions, which shorten the T1 relaxation time of surrounding tissue water and thereby increase MRI signal intensity in T1-weighted images.

The relatively simple but fundamental organization of insect brain has long been studied for a better understanding of the central nervous system in mammals. The antennal lobe of the sphinx moth *Manduca sexta* serves as a model for the olfactory system and its synaptic organization. The arrangement of the synaptic neuropil structures called olfactory glomeruli has been studied at different developmental stages covering the full range from P0 to P20. In particular, it has been reported that at pupal stage P12 the main wave of synaptogenesis in the antennal lobe is completed and that the glomeruli reached a dense synaptic pattern (Dubuque et al., 2001). Accordingly, intracellular recordings have shown that major synaptic activity becomes observable by P13 (Tolbert et al., 1983). The axons of the olfactory receptor neurons form a relatively long antennal nerve, which can be surgically perturbed before entering the antennal lobe. Disruption of the antennal nerve has served to elucidate olfactory signal processing under normal physiological conditions (Schachtner et al., 1999).

Extending a recent structural MRI study of the brain of *M. sexta* at different pupal stages (Michaelis et al., 2005), the purpose of this work was (i) to evaluate the feasibility of in vivo manganese-enhanced 3D MRI of *M. sexta*, and (ii) to investigate the functional responses in the two antennal lobes at pupal stages P13 to P17 which result from transection of one antenna at P12. Part of this work has appeared in abstract form (Watanabe et al., 2005).

* Corresponding author. Tel.: +49 551 201 1731; fax: +49 551 201 1307.
E-mail address: twatana@gwdg.de (T. Watanabe).

0165-0270/$ – see front matter © 2006 Elsevier B.V. All rights reserved.
doi:10.1016/j.jneumeth.2006.05.012

2. Materials and methods

2.1. Animals

M. sexta (Lepidoptera: Sphingidae) were reared as previously described (Schachtner et al., 2004). The pupal stage of a developing animal was determined according to established morphological changes and counted as P0 to P20 (Schachtner et al., 2004).

A total of 16 male pupae were included in the study. Twelve animals were studied between developmental stages P13 and P17. While four animals (#1 to #4) served as pure controls, eight animals (#5 to #12) were subjected to a transection of the right antenna at its base at P12. Two pupae (#5 and #6) served as sham-operated animals without the administration of $MnCl_2$. Six animals (#7 to #12) received an injection of an aqueous solution of $MnCl_2$ (20 μl, 20 mM) into the hemolymph near the proboscis within 24 h after the transection of the antenna, that is animal #7 at 0 h, animals #8 to #10 at 6 h, animal #11 at 20 h, and animal #12 at 24 h. Damage to the cuticle caused by the transection and injection was sealed with melted wax. Four younger male pupae (#13 to #16) were studied at P10/P11 to assess developmental influences on the manganese-induced MRI signal enhancement. These animals underwent the same procedures as animals #7 to #12 with the injection 6 h after transection.

All animals survived the transection of the antenna as well as the injection of manganese. The pupae developed until stage P20, which was followed by eclosion to normal-appearing adults with the wings darkly pigmented. Nevertheless, manganese is a neurotoxin and may affect neural activity at high concentrations. The chosen concentration of 20 mM was within the range previously used for functional brain studies. Here, the actual concentration reaching the brain was even lower as manganese was injected into the hemolymph.

2.2. MRI

The experimental setup was similar to a previous structural MRI study of the brain of *M. sexta* during metamorphosis (Michaelis et al., 2005). In particular, the pupa was fixed in a horizontal position which provides for natural physiologic conditions. Its head was positioned within a circular surface coil (10 mm inner diameter) used for MRI signal reception at optimum sensitivity. Homogeneous radiofrequency excitation was achieved with use of a large Helmholtz coil (100 mm inner diameter).

High-resolution 3D MRI was carried out at 2.35 T using a MRBR 4.7/400 mm magnet (Magnex Scientific, Abingdon, UK) and a DBX system (Bruker BioSpin MRI GmbH, Ettlingen, Germany) equipped with B-GA20 gradients (200 mm inner diameter, 100 mT m^{-1} maximum gradient strength). T1-weighted 3D MRI data sets with an isotropic resolution of 100 μm (FLASH, TR/TE = 20/7.8 ms, 25° flip angle, field-of-view (FOV) 12.8 mm × 25.6 mm × 25.6 mm, data acquisition matrix 128 × 256 × 256, 2 averages, 44 min measuring time, adapted from Natt et al., 2002) were repeatedly acquired between 0.5 and 45 h after manganese administration (the timings refer to the center of the measuring time). In selected cases, T1-weighted 3D MRI data sets were obtained with an isotropic resolution of 60 μm (FLASH, TR/TE = 20/8.1 ms, 25° flip angle, FOV 7.68 mm × 15.36 mm × 15.36 mm, matrix 128 × 256 × 256, 16 averages, 5 h 50 min measuring time).

2.3. Data evaluation

Cross-sectional images were obtained by multiplanar reconstructions from the original 3D MRI data sets in accordance with resolved anatomical structures. Subsequently, standardized regions-of-interest for the right and left antennal lobe were defined by manual drawing using a mouse-driven cursor in a horizontal section. An example is shown in Fig. 1. For quantitative evaluations, the SNR of an antennal lobe was determined by taking the mean MRI signal intensity within a respective region-of-interest divided by the standard deviation of the MRI signal intensity within a similarly sized region-of-interest outside the animal, that is within air. The percentage intra-individual SNR

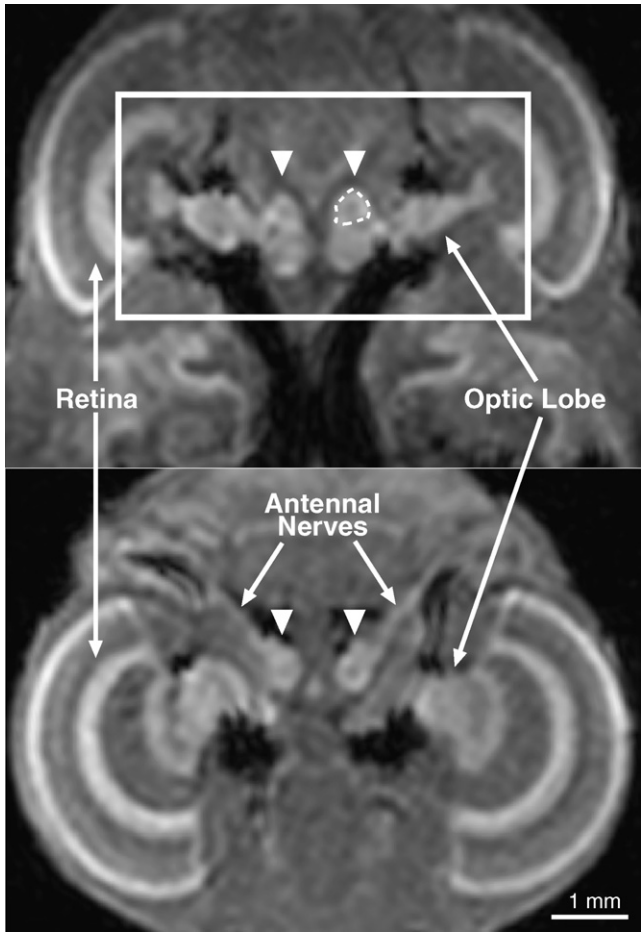

Fig. 1. (Top) Horizontal and (bottom) frontal section from a T1-weighted 3D MRI data set (3D FLASH, TR/TE = 20/7.8 ms, 25° flip angle, 100 μm isotropic resolution) of the brain of *M. sexta* (control animal #1) at stage P15 showing the antennal lobes (arrowheads), antennal nerves, optic lobes, and retina. The dashed line circumscribes a region-of-interest as used for SNR evaluations within the left antennal lobe. The white box refers to the zoomed areas shown in Figs. 2 and 4.

difference between the left antennal lobe and the right antennal lobe (with a transected antenna) was defined as the respective SNR difference divided by the SNR of the right antennal lobe and multiplied by 100.

Data expressed as mean ± S.D. were compared by analysis of variances (ANOVA) with post hoc comparisons either by Mann–Whitney *U*-test or Wilcoxon matched-pairs signed-ranks test. A p value < 0.05 was considered to be significant.

3. Results

As shown in Fig. 2, a pronounced MRI signal increase was observed in the functionally intact antennal lobe of P13 to P17 animals about 1 day after the systemic administration of manganese. On the other hand, such an enhancement was not seen in the antennal lobe of the transected side. These findings were independent of the time between transection and injection, and confirmed by a quantitative analysis. The antennal lobes of controls without transection of an antenna yielded a SNR of 24 ± 2 (4 data sets from animals #1 to #4). MRI performed at 20–24 h after manganese administration revealed a statistically significant SNR increase to 30 ± 5 ($p < 0.01$, 6 data sets from animals #7 to #12) in the antennal lobes of the intact left side corresponding to +22%. In contrast, a statistically not significant increase of 11% was observed in the right antennal lobe with a transected antenna.

In order to further separate functional enhancements from unspecific SNR increases in the antennal lobe of the transected side, differential enhancements were evaluated by comparing intra-individual SNR values of the right and left antennal lobe. As shown in Fig. 3, the data revealed a marked effect in favour of the left intact antennal lobe. Intra-individual SNR differences increased within 3 h after administration, reached a statistically significant level of 10 ± 5% at 20–24 h ($p < 0.05$, 6 data sets from animals #7 to #12), and remained elevated at least 2 days after administration.

It is of note that sham-operated pupae (animals #5 and #6) yielded differential SNR values of −2.5 and −1.6% at 35 and 50 h after transection of the right antenna, respectively. These findings indicate that the intervention itself did not interfere with the observed signal alterations. Additional control experiments were performed in younger pupae at stage P10/P11 (animals #13 to #16). In these cases, the intra-individual SNR differences were only 1 ± 4% for the intact lobe at 20–24 h after manganese administration (corresponding to 26–30 h after transection of the antenna). This lack of enhancement clearly supports the absence of any activity-related functional responses at this developmental stage.

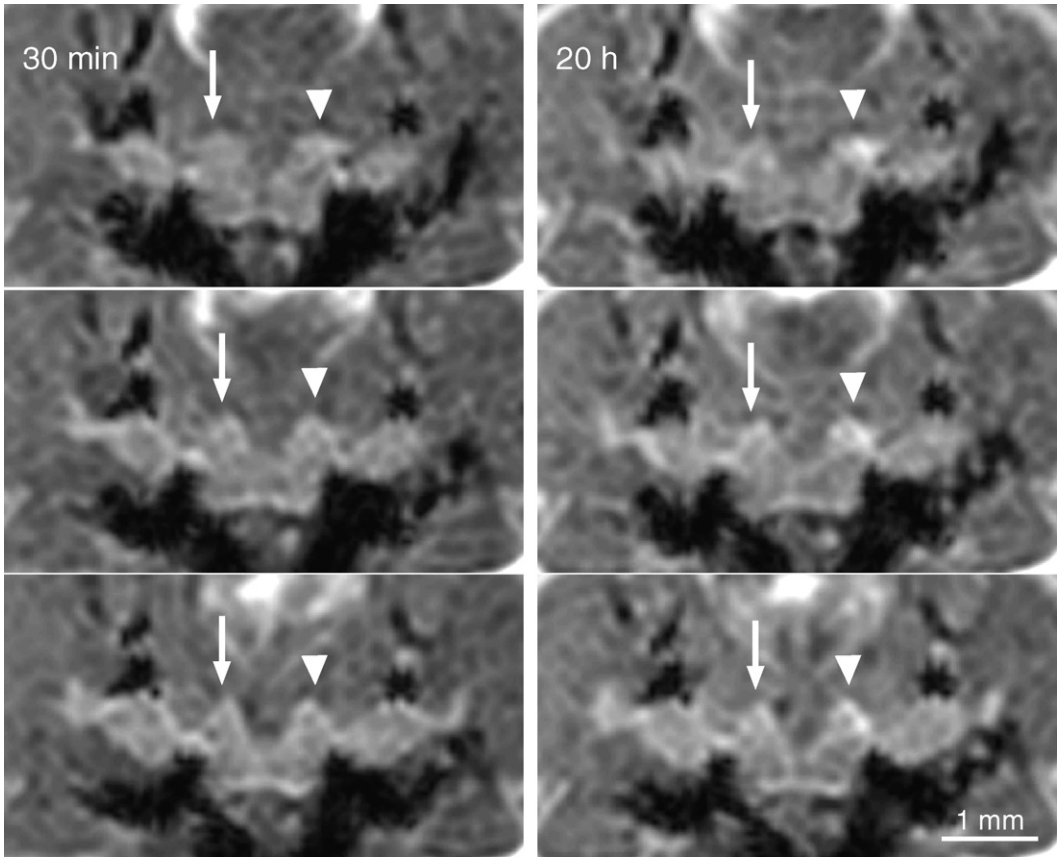

Fig. 2. Three contiguous horizontal sections from T1-weighted 3D MRI data sets (3D FLASH, 100 μm isotropic resolution) of the brain of animal #12 acquired (left) 30 min and (right) 20 h after the injection of $MnCl_2$ (20 μl, 20 mM) 24 h after transection of the right antenna at stage P13. A pronounced MRI signal increase is seen in the left antennal lobe (right arrowheads) served by an intact antenna, whereas a corresponding enhancement is not observed in the right antennal lobe (left arrows) after transection of its antenna.

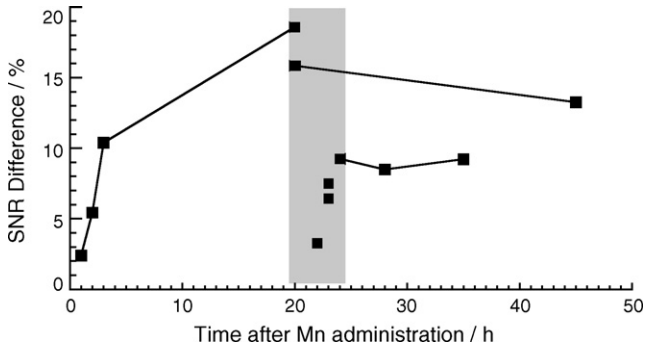

Fig. 3. Intra-individual SNR differences (in percent) between the left and right antennal lobe of pupae with transection of the right antenna as a function of time after manganese administration (12 data sets from animals #7 to #12). Connected squares refer to repeated MRI measurements of individual animals. The shaded area indicates the 20–24 h time window employed for statistical analyses (6 data sets from animals #7 to #12). In general, SNR differences between the antennal lobes occurred within 2–3 h after manganese injection and lasted for at least 2 days.

As demonstrated in Fig. 4 for animal #8 at P14, a more detailed morphological characterization of the antennal lobe was obtained by increasing the spatial resolution to 60 μm isotropic voxels. Although the achievable SNR of about 15 was slightly lower than for 3D MRI data sets at 100 μm isotropic resolution (Fig. 4, left), the resulting images clearly demonstrate that the MRI signal in the intact antennal lobe is not homogeneously increased. By reducing partial volume effects the enhanced ring-like structure at 100 μm resolution resolves into a more complex pattern at 60 μm resolution (Fig. 4, right). The spotty appearance of the manganese-enhanced structures agrees well with the described tissue arrangement at pupal stages P13 to P20 (Dubuque et al., 2001; Huetteroth and Schachtner, 2005). These bright structures are therefore supposed to represent the spheroidal alignment of the glomeruli. Accordingly, the pronounced accumulation of manganese along the glomeruli reflects the established synaptic transmission from the olfactory receptor neurons to the antennal lobe neurons.

4. Discussion

To the best of our knowledge, this study of the pupae of *M. sexta* is the first demonstration of manganese-enhanced MRI of insect brain. In a technical sense, the systemic administration of manganese into the hemolymph turned out to be feasible and robust. The observed variability of quantitative SNR increases across animals was not related to the time after transection or manganese administration and may be explained by inter-individual variations in the hemolymph system during pupal development between P13 and P17.

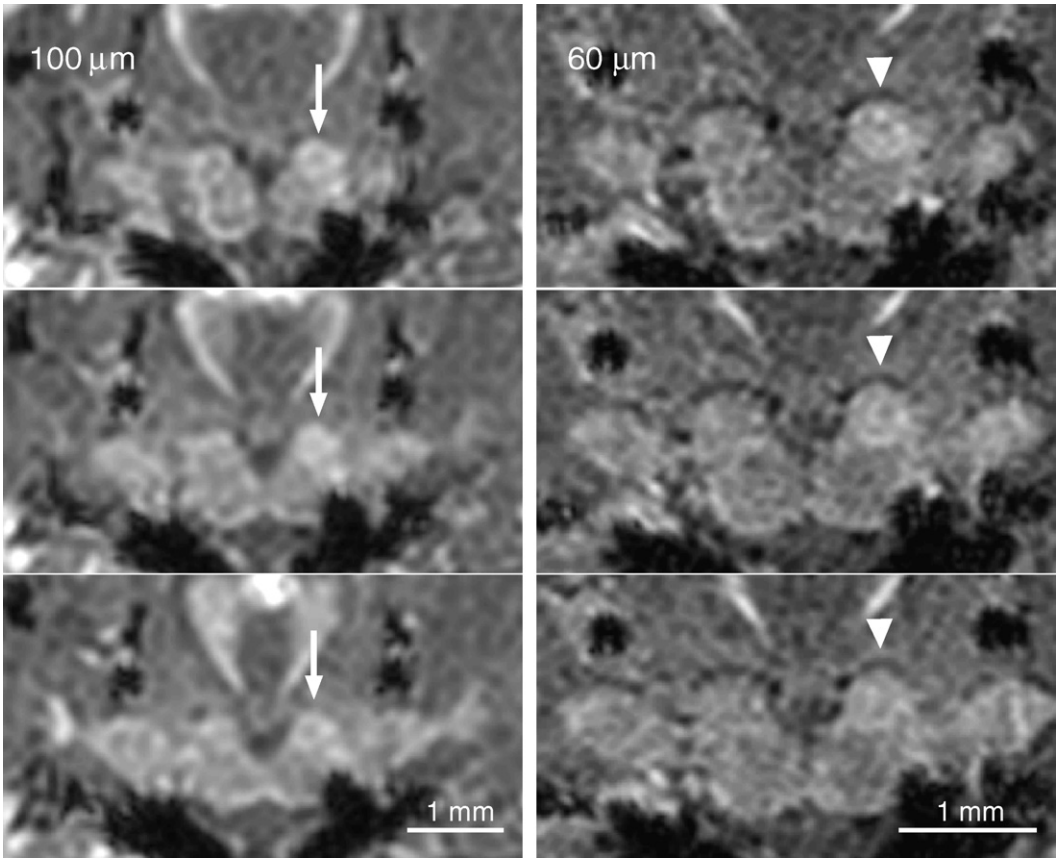

Fig. 4. Three contiguous horizontal sections from T1-weighted 3D MRI data sets (3D FLASH) of the brain of animal #8 depicting the antennal lobes 28 and 30 h after manganese administration at (left) 100 μm × 100 μm × 100 μm (1 nl) resolution and (right) 60 μm × 60 μm × 60 μm (0.216 nl) resolution. In this case $MnCl_2$ (20 μl, 20 mM) was injected 6 h after the transection of the right antenna at stage P14. The bright ring-like structure within the intact left antennal lobe detectable at 100 μm resolution (arrows) resolves into individual "hot spots" at 60 μm resolution (arrowheads).

Manganese ions are delivered to the brain via the systemic circulation and subsequently taken up by and accumulated within active neurons of the antennal lobes. In P13–P17 animals, the differential MRI signal enhancement in the functionally intact antennal lobe versus the lobe of the transected antenna agrees with the establishment of major synaptic connectivity by pupal stage P13 (Tolbert et al., 1983). More precisely, this finding supports the development of functional synapses between the spontaneously active olfactory receptor neurons and the neurons in the antennal lobes. Preliminary results at 60 μm isotropic resolution indicate that the manganese-enhanced ring-like substructures within the antennal lobe ("hot spots" in Fig. 4, right) coincide with the known locations of the glomeruli involved in odor processing. In view of the fact that the insect antennal system shares a basic organization with the olfactory system in vertebrates, it is interesting to note that the pronounced enhancement of the glomeruli is in line with previous observations in the olfactory system of mice (Watanabe et al., 2002) and rats (Aoki et al., 2004), where manganese appeared to accumulate in the glomerular layer of the olfactory bulb.

The significantly reduced uptake of manganese in the lobe of the transected antenna is intriguing in view of recent manganese-enhanced MRI studies of neural tissue under various perturbed conditions in rodents. For example, a manganese-induced enhancement was observed in brain regions suffering anoxic depolarization (Aoki et al., 2003), while diffuse and dispersed signal increases were observed in the hippocampal formation after kainic acid lesioning (Watanabe et al., 2004). Conversely, a lack of manganese-induced enhancement was found after radiation-induced axonal degeneration with demyelination (Ryu et al., 2002), in neural tissue distal to a nerve injury (Thuen et al., 2005; Bilgen et al., 2005), and in the auditory pathway after surgically induced hearing loss (Yu et al., 2005). In the case of *M. sexta*, transection of the antennal nerve has been shown to rapidly elicit electrical activity within antennal lobe neurons as monitored by cGMP upregulation (Schachtner et al., 1999). However, because the cGMP signal decreased to undetectable levels within 1 h, this damage-induced activity will not play a role in P13–P17 animals who received manganese at least 6 h after transection (animals #8–#12). The injection of manganese immediately after transection (animal #7) led to a similar signal behaviour. It should also be taken into account that the clear enhancement at 20–24 h after injection represents the manganese accumulated during the entire time period. The mild signal increase in the antenna-transected lobe is therefore expected to result from diffusion processes and/or residual uptake in line with similar unspecific SNR increases observed in the frontal cortex of mice after systemic application of manganese (Watanabe et al., 2002, 2004).

Taken together, the differential SNR increase in the intact antennal lobe of individual P13–P17 animals supports the notion that the spontaneous activity of the olfactory receptor neurons plays a predominant role in the uptake of manganese. Conversely, the much lower enhancement in the antenna-transected lobe must be associated with a functional disturbance. The MRI finding that the activity within the glomerular network of the antennal lobe disappears in the absence of spontaneous activity of the olfactory receptor neurons, favours the hypothesis that the spontaneous activity of the olfactory receptor neurons drives the major neuronal activity within the developing antennal lobe from P12. This understanding is further supported by the absence of a respective manganese-enhanced MRI signal in P10/P11 animals. At this earlier stage, olfactory receptor neurons already show spontaneous activity (Oland et al., 1996) and their axons have grown into the antennal lobe (Oland and Tolbert, 1996). Thus, the lack of a differential SNR increase in the intact antennal lobe at P10/P11 suggests that the synapses between the olfactory receptor neurons and the antennal lobe neurons are not yet fully functional despite reports of weak synaptic transmission starting from P9 (Tolbert et al., 1983). Accordingly, the MRI results support the view that functional synapses between olfactory receptor neurons and antennal lobe neurons are only established by pupal stage P13.

5. Conclusion

In summary, this study demonstrates the feasibility of manganese-enhanced MRI of insect brain in vivo. The observed preferential enhancement in the intact antennal lobe of P13–P17 animals is associated with the neuronal uptake of manganese from the hemolymph in response to spontaneous activity of olfactory receptor neurons. The significantly lower enhancement detected in the lobe of a transected antenna indicates a functional disturbance of the antennal system. The relationship between activity-related neuronal function and manganese-induced MRI signal enhancement is further supported by the lack of any preferential enhancement in the developing antennal lobe of P10/P11 animals. Manganese-enhanced MRI therefore allows for a structural as well as functional characterization of the olfactory system of insect brain in vivo. Further improvements of the spatial resolution will help to map odor-specific representations of glomerular activity in the olfactory system of insects under normal and altered physiological conditions.

References

Aoki I, Ebisu T, Tanaka C, Katsuta K, Fujikawa A, Umeda M, et al. Detection of the anoxic depolarization of focal ischemia using manganese-enhanced MRI. Magn Reson Med 2003;50:7–12.

Aoki I, Wu YJ, Silva AC, Lynch RM, Koretsky AP. In vivo detection of neuroarchitecture in the rodent brain using manganese-enhanced MRI. NeuroImage 2004;22:1046–59.

Bilgen M, Dancause N, Al-Hafez B, He YY, Malone TM. Manganese-enhanced MRI of rat spinal cord injury. Magn Reson Imaging 2005;23:829–32.

Brinkley CK, Kolodny NH, Kohler SJ, Sandeman DC, Beltz BS. Magnetic resonance imaging at 9.4 T as a tool for studying neural anatomy in nonvertebrates. J Neurosci Methods 2005;146:124–32.

Dubuque SH, Schachtner J, Nighorn AJ, Menon KP, Zinn K, Tolbert LP. Immunolocalization of synaptotagmin for the study of synapses in the developing antennal lobe of *Manduca sexta*. J Comp Neurol 2001;441:277–87.

Herberholz J, Mims CJ, Zhang X, Hu X, Edwards DH. Anatomy of a live invertebrate revealed by manganese-enhanced magnetic resonance imaging. J Exp Biol 2004;207:4543–50.

Huetteroth W, Schachtner J. Standard three-dimensional glomeruli of the *Manduca sexta* antennal lobe: a tool to study both developmental and adult neuronal plasticity. Cell Tissue Res 2005;319:513–24.

Koretsky AP, Silva AC. Manganese-enhanced magnetic resonance imaging (MEMRI). NMR Biomed 2004;17:527–31.

Michaelis T, Watanabe T, Natt O, Boretius S, Frahm J, Utz S, et al. In vivo 3D MRI of insect brain: cerebral development during metamorphosis of *Manduca sexta*. NeuroImage 2005;24:596–602.

Natt O, Watanabe T, Boretius S, Radulovic J, Frahm J, Michaelis T. High-resolution 3D MRI of mouse brain reveals small cerebral structures in vivo. J Neurosci Methods 2002;120:203–9.

Oland LA, Tolbert LP. Multiple factors shape development of olfactory glomeruli: insights from an insect model system. J Neurobiol 1996;30:92–109.

Oland LA, Pott WM, Bukhman G, Sun XJ, Tolbert LP. Activity blockade does not prevent the construction of olfactory glomeruli in the moth Manduca Sexta. Int J Dev Neurosci 1996;14:983–96.

Pautler RG. In vivo, trans-synaptic tract-tracing utilizing manganese-enhanced magnetic resonance imaging (MEMRI). NMR Biomed 2004;17:595–601.

Ryu S, Brown SL, Kolozsvary A, Ewing JR, Kim JH. Noninvasive detection of radiation-induced optic neuropathy by manganese-enhanced MRI. Radiat Res 2002;157:500–5.

Schachtner J, Homberg U, Truman JW. Regulation of cyclic GMP elevation in the developing antennal lobe of the sphinx moth *Manduca sexta*. J Neurobiol 1999;41:359–75.

Schachtner J, Huetteroth W, Nighorn A, Honegger HW. Copper/zinc superoxide dismutase-like immunoreactivity in the metamorphosing brain of the sphinx moth *Manduca sexta*. J Comp Neurol 2004;469:141–52.

Thuen M, Singstad TE, Pedersen TB, Haraldseth O, Berry M, Sandvig A, et al. Manganese-enhanced MRI of the optic visual pathway and optic nerve injury in adult rats. J Magn Reson Imag 2005;22:492–500.

Tolbert LP, Matsumoto SG, Hildebrand JG. Development of synapses in the antennal lobes of the moth *Manduca sexta* during metamorphosis. J Neurosci 1983;3:1158–75.

Watanabe T, Natt O, Boretius S, Frahm J, Michaelis T. In vivo 3D MRI staining of mouse brain after subcutaneous application of $MnCl_2$. Magn Reson Med 2002;48:852–9.

Watanabe T, Frahm J, Michaelis T. Functional mapping of neural pathways in rodent brain in vivo using manganese-enhanced three-dimensional MRI. NMR Biomed 2004;17:554–68.

Watanabe T, Schachtner J, Krizan M, Boretius S, Frahm J, Michaelis T. Observation of neural activity in insect brain in vivo using Mn^{2+}-enhanced 3D MRI. Proc Intl Soc Mag Reson Med 2005;13:1005.

Yu X, Wadghiri YZ, Sanes DH, Turnbull DH. In vivo auditory brain mapping in mice with Mn-enhanced MRI. Nat Neurosci 2005;8:961–8.